FEBS Letters 585 (2011) 3139–3145

journal homepage: www.FEBSLetters.org

Human topoisomerase II–DNA interaction study by using atomic force microscopy

Livan Alonso-Sarduy [a,*], Charles Roduit [a], Giovanni Dietler [a], Sandor Kasas [a,b]

[a] Laboratoire de Physique de la Matière Vivante, École Polytechnique Fédérale de Lausanne (EPFL), CH-1015 Lausanne, Switzerland
[b] Département de Biologie cellulaire et de Morphologie, Université de Lausanne (UNIL), CH-1015 Lausanne, Switzerland

ARTICLE INFO

Article history:
Received 25 April 2011
Revised 24 August 2011
Accepted 31 August 2011
Available online 6 September 2011

Edited by Michael R. Bubb

Keywords:
AFM
DNA topology
Human topoisomerase II
Binding geometry
Time-lapse imaging
Protein–DNA interaction

ABSTRACT

Type II topoisomerases (Topo II) are unique enzymes that change the DNA topology by catalyzing the passage of two double-strands across each other by using the energy from ATP hydrolysis. In vitro, human Topo II relaxes positive supercoiled DNA around 10-fold faster than negative supercoiled DNA. By using atomic force microscopy (AFM) we found that human Topo II binds preferentially to DNA cross-overs. Around 50% of the DNA crossings, where Topo II was bound to, presented an angle in the range of 80–90°, suggesting a favored binding geometry in the chiral discrimination by Topo II. Our studies with AFM also helped us visualize the dynamics of the unknotting action of Topo II in knotted molecules.
© 2011 Federation of European Biochemical Societies. Published by Elsevier B.V. All rights reserved.

1. Introduction

Topoisomerases are enzymes that can change the DNA topology, either by over- and under-winding of DNA molecules or by helping to unravel the knots and tangles from the genetic material, and thereby facilitating gene expression, cell division, transcription, duplication [1], etc. Topoisomerases relax DNA either by passing one single-strand of a DNA fragment through the opposing one (type I subfamily) or by passing one double-stranded segment (the transfer- or T-segment) through a temporary break formed in another one (the gate- or G-segment) which belong to the same or different molecules (type II subfamily) [1,2].

The present study focuses on the action of human Topo II. Two main questions arise when studying the action of Topo II: the first relates to where Topo II bind to. According to some studies, the binding mechanism of Topo to DNA could be determined towards preferred sequence sites and not at random locations [3]. However, recent studies have shown that the mechanism by which Topo II select DNA sites is not clear and the specificity of Topo II-mediated cleavage is determined by the local conformation of the DNA that accompanies the sequence, as opposed to a direct recognition of the bases that the sequence contains [4]. On the other hand, in vitro experiments have shown that human Topo II and Topoisomerase IV (Topo IV) relax positive supercoiled DNA faster than negative supercoiled DNA [5,6]. Recent theoretical results explain this chiral discrimination suggesting that Topo IV bind to DNA strands juxtaposed in a nearly perpendicular orientation [7]. The second question relates to the selection of strand passages performed by Topo II, which has been shown to be non-random and directed towards unknotting of DNA knots [8]. The size of a Topo II molecule does not allow it to recognize the global topology of a much larger molecule (DNA). Therefore it has been proposed that the local information pertaining to the juxtaposition of two DNA strands might reflect the global topology and be used by Topo II to favour unknotting. Many ideas have been proposed and numerical simulations have been implemented to prove or disprove the hypothesized mechanisms [9–13]. Moreover, experiments on supercoiled, catenated or knotted DNAs have been carried out under controlled conditions [14,15].

In the present letter, we use AFM [16] to study the action of topoisomerases on knotted DNA in air and in a liquid environment. This technique permits nanometric-scale imaging of single molecules under near-physiological conditions, advantage that has already been used to study the dynamics of different biological processes [17–20]. In the present case, this method allowed us to study the binding of human Topo II to DNA. Moreover, we show here that a mild attachment of DNA molecules on the imaging substrate made it possible to follow the topological evolution of the molecules in time.

Abbreviations: AFM, atomic force microscopy; Topo II, type II topoisomerases; Topo IV, Topoisomerase IV

* Corresponding author. EPFL SB IPSB LPMV, BSP 411, CH-1015 Lausanne, Switzerland. Fax: +41 21 69 30422.
E-mail address: livan.alonso@epfl.ch (L. Alonso-Sarduy).

0014-5793/$36.00 © 2011 Federation of European Biochemical Societies. Published by Elsevier B.V. All rights reserved.
doi:10.1016/j.febslet.2011.08.051

2. Material and methods

2.1. DNA substrates, enzymes and reagents

Negative supercoiled pBR322 plasmid DNA (4361 base-pairs) was purchased from Fermentas and human Topo II α p170 from TopoGEN. Magnesium chloride hexahydrate, sodium chloride, nickel chloride hexahydrate, DTT and EDTA (all with analytical grade) were supplied by Sigma–Aldrich.

Linear DNA fragments (251 and 537 bp) were amplified from pBR322 by PCR using 4 primers: 5′ CGGATTCACCACTCCAAGAA 3′, 5′ TTCACGTTCGCTCGCGTAT 3′, 5′ GTTTCGGTGATGACGGTGA 3′ and 5′ TATAGTCCTGTCGGGTTTCG 3′; subsequently separated on 2.5% agarose gels, purified using a QIAprep Spin MiniPrep Kit (QIAGEN) and extracted using phenol:chloroform:isoamyl alcohol (25:24:1, SIGMA).

2.2. Isolation of knotted DNA from tailless P4 capsids

Knotted DNA and nicked knotted DNA were produced according to the protocol described by Trigueros et al. [21] and Zhang et al. [22], respectively.

2.3. Preparation of Topo II–DNA complexes

All complexes were prepared in tubes prior to deposition onto the mica surface for AFM imaging in air. Human Topo II (10–250 nM) were incubated with pBR322 (200 nM) or linear DNA fragments (10–100 nM), for 5–30 min at 30 °C, in the working buffer (see Table S1).

2.4. Atomic force microscopy

Before deposition of the complexes onto the surfaces, unless stated otherwise, $NiCl_2$ at final concentration ranging from 0.1 to 1 mM was added to the solution. Subsequently, mixture was adsorbed onto the freshly cleaved mica (Pelco Mica, Ted Pella Inc., Redding, CA) and incubated thereon for 1–5 min. The mica surface was then rinsed with pure water, blow drying it with compressed air and imaged by AFM in air.

For the in situ AFM imaging, freshly cleaved mica was pre-treated with a 10 μl drop of 1 mM $NiCl_2$ for 2 min. After rinsing it with ultra-pure water and blow drying it with compressed air, 10 ng of knotted DNA molecules (diluted in a solution containing 10 mM Tris–HCl (pH 8.0), 2 mM $MgCl_2$ and 10 mM NaCl), Topo II–DNA complexes or human Topo II (200 nM) were deposited on the nickel-treated mica. For time-lapse AFM imaging a mixture of human Topo II (200 nM) and ATP solution (20 mM) was injected into the fluid chamber for starting the reaction.

In each case, the sample was covered with a glass imaging chamber (Bruker, Santa Barbara, CA). AFM images were collected using a MultiMode SPM with a Nanoscope III controller (Bruker, Santa Barbara, CA), operated in tapping-mode and acquired at a rate of 1 or 4 lines/s. Silicon nitride cantilevers (Bruker, Santa Barbara, CA) with a typical tip radius below 10 nm (spring constant: 5 N/m) were used for imaging in air; and cantilevers with a typical tip radius around 10 nm (spring constant: 0.32 N/m) were used for imaging in liquid. Typical tapping frequency was between 7 and 12 kHz.

Images were simply flattened using the Nanoscope III software (Version 5.31, Bruker), and no further image processing was carried out.

2.5. Injection system

Different imaging buffers were assayed using a flow apparatus [23]. 400 μl of each buffer were injected at a flow rate of 40 μl/min, the volume being sufficient to effect a complete exchange of the fluid.

Table S1 gives the chemical concentrations of the imaging buffers. These 3 buffers are needed in order to permit attachment and detachment of the DNA molecules and more importantly to observe the activity of the Topo II.

2.6. DNA relaxation and gel electrophoresis

DNA relaxation assays were performed as described by McClendon et al. [6].

The samples were electrophoresed in 1% agarose containing 100 mM Tris–borate (pH 8.3) and 2 mM EDTA. The gels were stained with ethidium bromide (0.5 μg/ml) for 30 min. The DNA bands were visualized with ultraviolet light and quantified using a Kodak® 1D Image Analysis Software.

2.7. Crossing angle and radius of gyration of DNA molecules

The DNA crossing angle, extracted from the Topo II-linear DNA complexes images, was measured using the Ellipse modular software package (ViDiTo, Kosice, Slovakia; www.vidito.com).

The sizes of the DNA molecules were gauged by determining the radius of gyration. The square radius of gyration (R_g^2) is defined as the average square distance between monomers in a given conformation (position vector $\vec{R}_i$) and the polymer's centre of mass (position vector $\vec{R_{cm}} = \frac{1}{N}\sum_{i=1}^{N}\vec{R}_i$):

$$R_g^2 = \frac{1}{N}\sum_{i=1}^{N}\left(\vec{R}_i - \vec{R_{cm}}\right)^2$$

We used our own MATLAB image-analysis program to analyse the complex shapes of the knotted DNA molecules (see Supplementary data, Fig. S1a–d). The algorithms that were derived from the image analysis permitted us to calculate the radius of gyration.

2.8. Statistical analysis

Data are presented as mean ± standard deviation. Student's t test (two-tailed) was used to compare two groups ($P < 0.05$ was considered significant).

3. Results and discussion

3.1. Human Topo II bind to DNA cross-overs

Topo II seems to proceed to a selection of DNA segment juxtapositions. However, it is still unclear if it directly binds to a segment juxtaposition or if it first binds to the G-segment and then selects the correct T-segment. To address this question, human Topo II were incubated with pBR322 and after addition of $NiCl_2$, the sample was deposited onto the mica and imaged using AFM in air. Analysis of cross-sections profiles of AFM topographical images of double-stranded DNA, DNA crossings, Topo II, and Topo II–DNA complexes, allowed us to distinguish between DNA crossings and Topo II molecules (see Supplementary data, Fig. S2a–d). We analysed 256 complexes and we found that 90.7 ± 2.4% of human Topo II were bound at points of helix–helix juxtaposition on DNA plasmids (Fig. 1); similar results have been found for *Drosophila* and calf thymus Topo II [24], however Topo IV from *E. coli* and yeast Topo II were localized at the supercoiled DNA apices [10]. On the other hand, several models suggest that Topo II directly bind to DNA crossings. For example, numerical studies have suggested that Topo II preferentially bind to hooked juxtapositions, which are encountered frequently in the supercoiled and knotted portions, therefore promoting unwinding and unknotting of DNA [12,13].

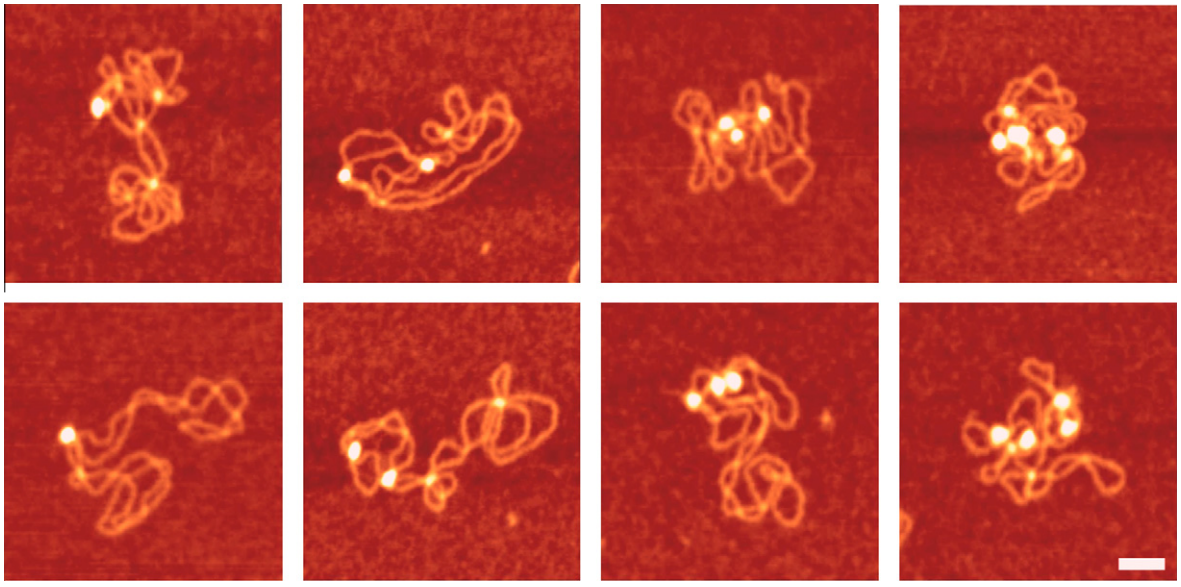

Fig. 1. Topo II recognition of DNA cross-overs in supercoiled plasmids. Human Topo II (53.92 nM) were incubated with pBR322 and imaged by AFM in air. Representative micrographs of different numbers of human Topo II molecules bound to plasmid DNA are shown. The bar represents 50 nm.

Under appropriate ionic conditions, the Topo II–DNA complex forms rapidly and the stoichiometry of the interaction should depend on the concentration of the enzyme. We analyzed AFM images to quantify the association of Topo II with DNA and to determine the amount of bound Topo II molecules per DNA molecule. As expected, increasing the concentration of Topo II increases the probability to have more than one bound Topo II per DNA molecule (Fig. 2). Additionally, we found that for different concentrations of Topo II, the percentage of Topo II bound to helix–helix juxtapositions on DNA plasmids was kept around 90%. Moreover, in most of the cases there is one Topo II molecule bound at one crossover, but we have observed cases in which more than one are bound to one DNA cross-over (Fig. S3).

3.2. Human Topo II bind to linear DNA fragments in absence of torsional constraints

According to the previously described study it seems that human Topo II recognizes DNA cross-overs preferentially. To confirm that Topo II may recognize DNA nodes even though they are not under torsional constraints, the interaction between Topo II and linear DNA fragments was explored. Firstly, linear DNA fragments were amplified by PCR from pBR322 with sizes of 251 and 537 bp. The small size of the linear DNA fragments was chosen to allow them to have bigger flexibility during adhesion and immobilization on mica surfaces.

Similar experiments to those described with negative supercoiled plasmid and Topo II were carried out using linear DNA fragments (100 nM). Topo II were observed at DNA cross-overs on linear DNA fragments in 27.3 ± 2.5% of the 301 scored complexes (Fig. 3a). While these percentages are somewhat lower than those generated with partially supercoiled circular plasmids, the incidence of cross-overs observed with linear DNA molecules in the absence of Topo II was of only 6.0 ± 1.2%. This finding suggests that recognition was independent of torsional stress, since enzyme molecules were also found at cross-overs on linear DNA fragments as shown in Fig. 3a. Same experiments using lower concentration of linear DNA fragments (20 nM) showed that Topo II were observed at DNA cross-overs on linear DNA fragments in 26.1 ± 2.1% of the 214 scored complexes, a similar value to the one obtained previously; however, the incidence of cross-overs

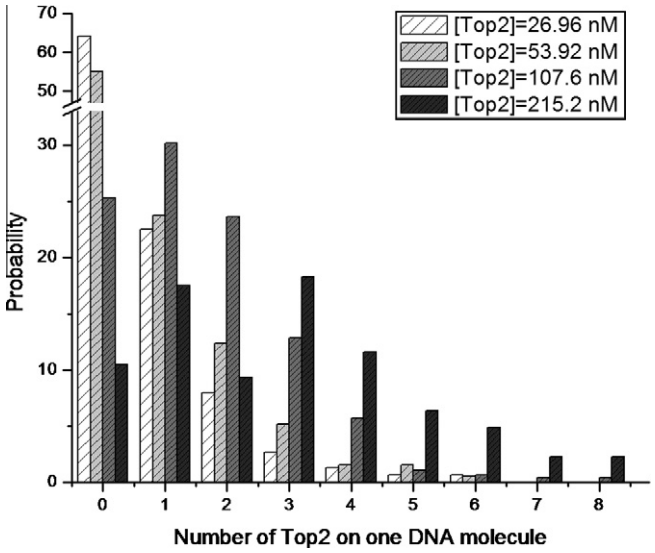

Fig. 2. Quantization of protein occupancy on DNA molecules at different concentrations of Topo II derived from AFM images. Human Topo II were incubated with pBR322 and imaged by AFM in air.

observed with linear DNA molecules in the absence of Topo II decreased from 6.0 ± 1.2 to 2.3 ± 0.6%. This result shows that the decrease of the concentration of linear DNA fragments and thus the number of points of helix–helix juxtaposition on DNA does not reduce the number of Topo II bound to DNA cross-overs, keeping their preferential binding to these regions. Added to this, the high proportion of Topo II bound at DNA cross-overs suggests this mechanism as preferential compared to a sequential binding to G- and T-segments.

3.3. Human Topo II bind to DNA cross-over at specific angle

One specific feature of bacterial Topo IV and human Topo II is their preferential relaxation of positive vs. negative supercoils [5,6]. The most straightforward explanation of this preference is the recognition of specific G- and T-segment arrangements by

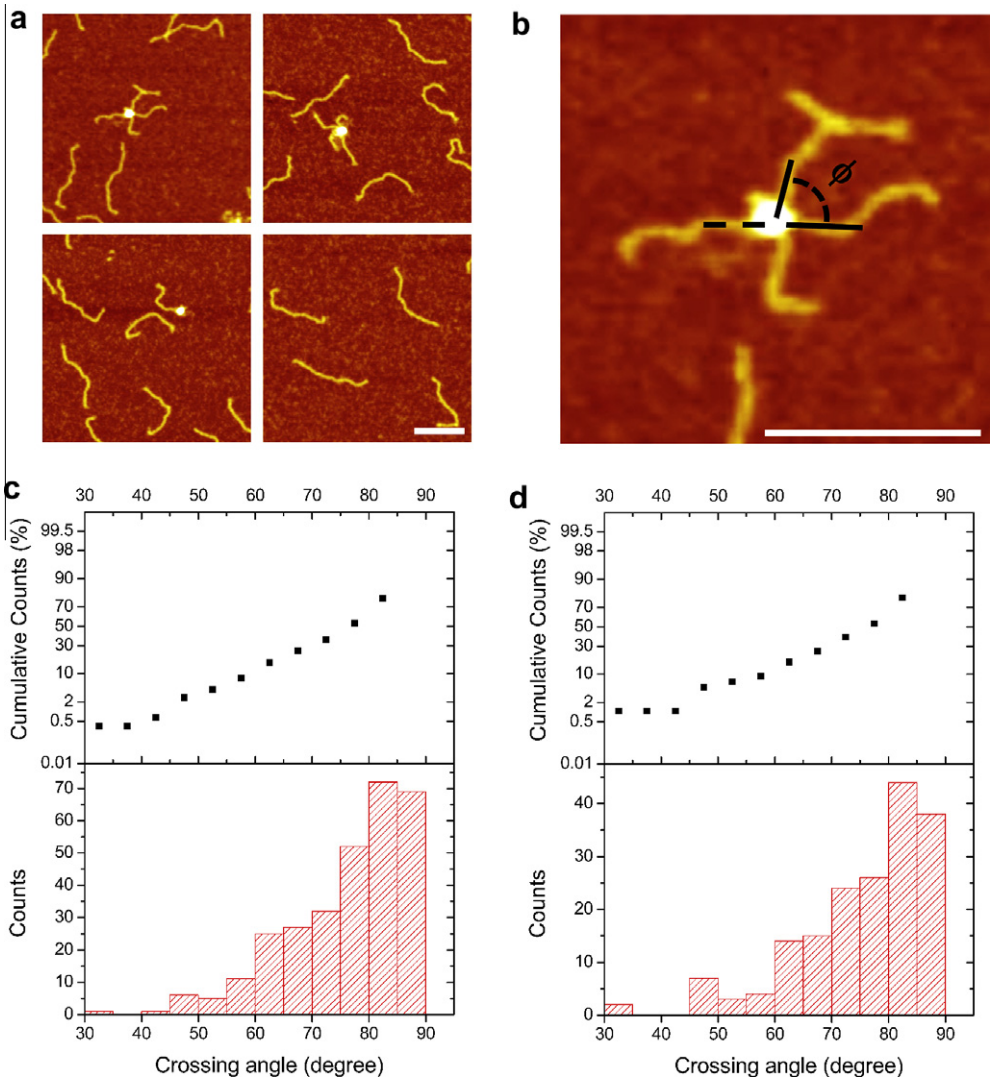

Fig. 3. Topo II bind to DNA cross-overs on linear DNA molecules with a specific geometry. Human Topo II (53.92 nM) were incubated with linear DNA fragments (100 nM). After addition of 1 mM of $NiCl_2$ (a–c) or 1 mM of $MgCl_2$ (b) to the solution, mixture was adsorbed to mica and imaged by AFM in air. (a) Representative micrographs of one Topo II in complex with DNA cross-overs (top panel) and with a linear DNA fragment (left bottom panel) are shown at a higher magnification; linear DNA fragments are shown in the right bottom panel. (b) A representative micrograph of Topo II bound to a DNA cross-over complex with the measured angle ϕ is indicated. (c, d) Distribution of crossing angle ϕ is determined by semi-automated method. The bar represents 100 nm.

the enzyme. A structural constraint that would increase the affinity of Topo II for left-handed crossings would therefore rationalize the substrate-dependent activity of Topo.

We calculated the crossing angle between two segments of DNA fragments bound to Topo II in different ionic conditions (Fig. 3a–d). Since we were not able to determine from the AFM images which strand passes on top of the other, we could not define the chirality of the crossing. Therefore, we defined the crossing angle as the smallest necessary rotation to bring the fragments in parallel orientation. Around 50% of the fragment cross-overs presented an angle between the two DNA fragments in the range 80–90° (Fig. 3c and d), indicating that, independently from the chirality, Topo II predominantly binds to large crossing angles.

We noticed that the presence of 0.1–1 mM $NiCl_2$ in the buffer, increased the population of Topo II–DNA complexes in a similar manner as it has been described for Ca [25]. However, this parameter did not affect the measured crossing angle as depicted in Fig. 3c and d.

Our results corroborate previous ones where, by using single-molecule techniques with DNA braids, it was shown that the difference in the relaxation activity could be partially attributed to a different processivity of Topo IV on positive and negative supercoils [7,26]. Since Topo II are much more processive on positive supercoils, the crossing angle discrimination would not have to be so strong and even the crossing angle 82.5° (most probable crossing angle obtained from the distribution), close to the achiral angle of 90°, would allow for sufficient discrimination.

3.4. In situ AFM imaging under aqueous liquid environment

We used AFM to follow the action of Topo II on DNA molecules in solution without drying, i.e., AFM in situ, in order to directly observe the Topo II–DNA interactions at the single molecule level. Generally, AFM imaging in liquid requires the sample (DNA in our case) to be fixed to a flat substrate (mica in our case) with sufficient strength to prevent its detachment by the scanning tip. At the same time, the sample must be bathed by a medium that not only allows interaction between ligands and DNA molecules, but also that neither influences the topology of the latter nor interferes with the activity of the former. Additionally, it should be taken into account that the Mg^{2+}/Na^{+} ratio is crucial for the establishment of optimal DNA–imaging conditions [27]. To modulate the degree of

DNA freedom during imaging, buffers containing different concentrations of Mg^{2+} and Na^{+} were injected into the observation chamber (Supplementary data, Fig. S4, Video S1). The activity of Topo II was preserved in these buffers, as can be seen in the gel (Fig. S5a–d).

We started by imaging native Topo II in liquid to determine its overall shape in physiological conditions. In addition to deforming DNA, Topo II undergo substantial conformational changes before and during its binding to the substrate. We could observe the homodimers of Topo II in liquid (Fig. 4a and b), whose conformations can be splitted into two groups: closed and opened. These data are in good agreement with the models proposing that Topo II adopts different conformations during its catalytic cycle [28,29]. Also, two main domains can be distinguished in each monomer (around 15 nm each) which could correspond with ATPase and DNA binding regions of Topo II. The apparent dimensions of Topo II molecules determined by AFM (major and minor axes provide solid estimation of the lengths and widths distribution of the particles: 30 ± 6 nm × 17 ± 4 nm) are similar to those obtained in air, but typically larger than their expected crystallographic dimensions (15–19 × 10–14 nm) [28–30]. This phenomenon could be explained by the force exerted by the AFM tip that flattens the sample and/or the convolution of the shape of the tip with the shape of the molecule. Based on these factors, the dimensions for Topo II obtained by AFM are within the expected range. We present what to our knowledge are the first images of human Topo II in physiological conditions; previous studies have been carried out, in dried conditions, by using electron microscopy and AFM [31,32].

Many of the biological samples suitable for imaging AFM are subject to artefacts if they are dried. This could explain the shape differences that we have observed between AFM imaging experiments in air, where we observed that Topo II showed an ellipsoidal shape (Fig. 1, Fig. S2b), and in liquid, where we observed that Topo II molecules adopt a well-defined homodimer structure (Fig. 4a and b). Additionally, we checked the Topo II–DNA complexes in liquid and we observed that Topo II conserved its natural structure (compare Fig. 4a–c). Those results revealed that the morphology of the adsorbed protein was altered depending of the imaging conditions.

3.5. Time-lapse AFM imaging of knotted DNA relaxation induced by human Topo II in liquid

After having observed the Topo II–DNA complexes in a static way, we implemented experiments to assess the in situ effect of Topo II activity on a single knotted molecule of DNA. In this set of experiments, knotted species of circular DNA were used as reporters of Topo II activity. When knotted DNA molecules are adsorbed onto a surface, the number of crossings will depend upon the knot complexity and the degree of supercoiling. To eliminate the confounding effects of crossings due to supercoiling, nicked knotted DNA molecules were prepared. Then, we deposited the nicked knotted DNA molecules on nickel-treated mica and sample was placed on the microscope. At this moment Topo II has not been injected into the fluid chamber and the white dots observed on Fig. 5a top panel, correspond to the knots on the DNA molecules. Subsequently we injected a mixture of human Topo II and ATP solution into the fluid chamber for starting the reaction ($t = 0$). It is well known that the presence of ATP can trigger DNA relaxation (Fig. S5a–c). Our experiment has permitted, for the first time, a monitoring of the dynamics of DNA unknotting by Topo II (Fig. 5a; Video S2). The process of relaxation was completed within 200 s, after which the enzyme was dissociated from the DNA molecule. In the lower panel of images in Fig. 5a, several segments of the DNA molecule are invisible, probably as a result of a local desorption from the mica surface.

The activity of human Topo II from many image sequences similar to the one in Fig. 5a, was quantified by determining the radius of gyration of DNA molecules (Fig. 5b). The radius of gyration can be used to describe the size of any polymer, irrespective of its architecture, including branched and circular structures in which the end-to-end distances are ill-defined. Indeed, the global size of a polymer is drastically affected by topology, complex knots being more compact than simple knots. In our experiments, before the injection of Topo II and ATP ($t < 0$), the radii of gyration of knotted DNA molecules were of comparable value (190 ± 28 nm), indicating no effects of imaging buffers on DNA conformations (Fig. 5a). Immediately, after Topo II and ATP injection, a two-fold increase was observed upon unknotting of the DNA molecules (370 ± 32 nm, $P < 0.005$). Interestingly, following our single molecule experiments, the addition of Topo II lead to DNA unknotting activity, but never to DNA knotting (Fig. 5a).

One limiting factor of a conventional AFM operation is the speed at which images can be acquired. Due to the low temporal resolution of our AFM in liquid, we were not able to follow single Topo II molecules, moving on the surface or along the DNA, and this is one of the required conditions to answer this question by AFM. Thermal diffusion and flow of liquid (during the exchange of buffers) contribute to Topo II movement and its release off the surface. However, it is noteworthy that the resolution was enough to follow the dynamics of the conformational changes induced by the enzyme on the DNA molecules. The new available high-speed AFMs [33–35] should clarify the mechanism of binding of Topo II to DNA molecules.

4. Summary

Our experimental evidences allow us to confirm that human Topo II bind preferentially to DNA cross-overs with a specific geometry. Using time-lapse AFM in liquid, we monitored the structural and conformational changes during the unknotting activity of Topo II, providing further evidence of the coordinated mechanism

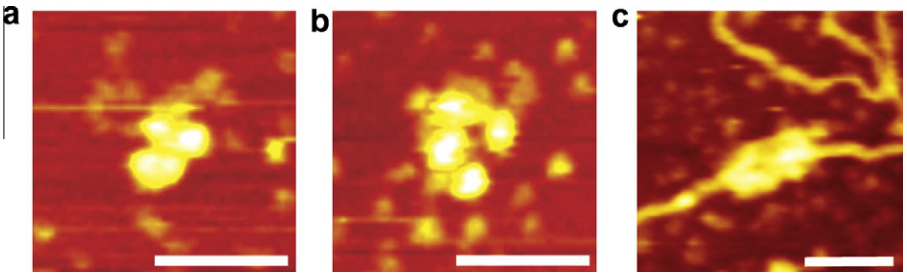

Fig. 4. (a, b) AFM imaging of two representative human Topo II conformations in liquid. (c) Human Topo II (53.92 nM) were incubated with pBR322. Mixture was adsorbed to nickel-treated mica and imaged by AFM in liquid. AFM imaging of a representative human Topo II–DNA complex in liquid (in this case two Topo II molecules are bound at the same position, possibly indicating cooperative behaviour). The bar represents 40 nm.

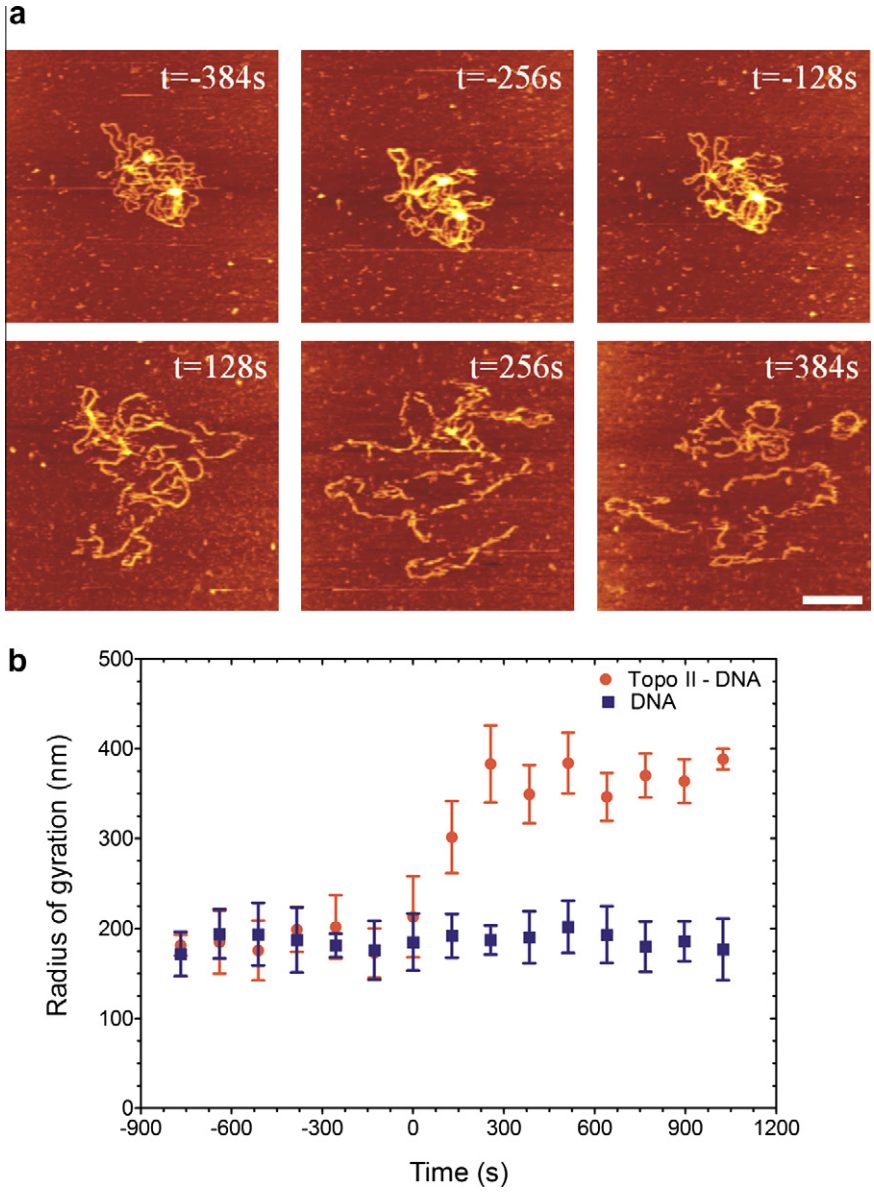

Fig. 5. (a) Nanoscale time-lapse imaging of the Topo II-induced unknotting on a representative single DNA molecule, which had been adsorbed to nickel-treated mica and imaged in liquid. The times lapses after the injection of 5 μl of human Topo II (215.2 nM) and 5 μl of ATP (20 mM) into the imaging chamber (t = 0) are indicated in seconds. During the course of the experiment, buffers containing different concentrations of Mg^{2+} and Na^{+} were injected into the imaging chamber (see Supplementary data, Table S1): working buffer between −384 s and −128 s; detaching buffer between −128 s and +128 s; and attaching buffer between +128 s and +384 s. The bar represents 250 nm. (b) Temporal course of Topo II-induced changes in the radius of gyration of DNA molecules during the unknotting process. Each data point represents the mean ± S.D. of radius of gyration of knotted DNA molecules treated (n = 8, red circle) and non-treated (n = 4, blue square) with Topo II. The complete transition from knotted to unknotted DNA form takes place, under the present conditions, in less than 200 s.

of action of Topo II. Together, the aforementioned data provide a framework for understanding the mechanistic feature of this reaction and the conformational changes that it implies.

Acknowledgements

This work was supported by a grant from the Swiss National Science Foundation (nos.: 200020-131865). We thank Dr. Andrzej Stasiak, Dr. Guillaume Witz, Dr. Jozef Adamcik and the members of our laboratory for many helpful discussions.

Appendix A. Supplementary data

Supplementary data associated with this article can be found, in the online version, at doi:10.1016/j.febslet.2011.08.051.

References

[1] Wang, J.C. (2002) Cellular roles of DNA topoisomerases: a molecular perspective. Nat. Rev. Mol. Cell Biol. 3, 430–440.
[2] Champoux, J.J. (2001) DNA topoisomerases: structure, function, and mechanism. Annu. Rev. Biochem. 70, 369–413.
[3] Capranico, G. and Binaschi, M. (1998) DNA sequence selectivity of topoisomerases and topoisomerase poisons. Biochim. Biophys. Acta 1400, 185–194.
[4] Velez-Cruz, R., Riggins, J.N., Daniels, J.S., Cai, H., Guengerich, F.P., Marnett, L.J. and Osheroff, N. (2005) Exocyclic DNA lesions stimulate DNA cleavage mediated by human topoisomerase II alpha in vitro and in cultured cells. Biochemistry 44, 3972–3981.
[5] Crisona, N.J., Strick, T.R., Bensimon, D., Croquette, V. and Cozzarelli, N.R. (2000) Preferential relaxation of positively supercoiled DNA by *E. coli* topoisomerase IV in single-molecule and ensemble measurements. Genes Dev. 14, 2881–2892.
[6] McClendon, A.K., Rodriguez, A.C. and Osheroff, N. (2005) Human topoisomerase IIalpha rapidly relaxes positively supercoiled DNA:

implications for enzyme action ahead of replication forks. J. Biol. Chem. 280, 39337–39345.
[7] Neuman, K.C., Charvin, G., Bensimon, D. and Croquette, V. (2009) Mechanisms of chiral discrimination by topoisomerase IV. Proc. Natl. Acad. Sci. USA 106, 6986–6991.
[8] Rybenkov, V.V., Ullsperger, C., Vologodskii, A.V. and Cozzarelli, N.R. (1997) Simplification of DNA topology below equilibrium values by type II topoisomerases. Science 277, 690–693.
[9] Witz, G. and Stasiak, A. (2010) DNA supercoiling and its role in DNA decatenation and unknotting. Nucleic Acids Res. 38, 2119–2133.
[10] Vologodskii, A.V., Zhang, W.T., Rybenkov, V.V., Podtelezhnikov, A.A., Subramanian, D., Griffith, J.D. and Cozzarelli, N.R. (2001) Mechanism of topology simplification by type II DNA topoisomerases. Proc. Natl. Acad. Sci. USA 98, 3045–3049.
[11] Burnier, Y., Dorier, J. and Stasiak, A. (2008) DNA supercoiling inhibits DNA knotting. Nucleic Acids Res. 36, 4956–4963.
[12] Liu, Z.R., Mann, J.K., Zechiedrich, E.L. and Chan, H.S. (2006) Topological information embodied in local juxtaposition geometry provides a statistical mechanical basis for unknotting by type-2 DNA topoisomerases. J. Mol. Biol. 361, 268–285.
[13] Witz, G., Dietler, G. and Stasiak, A. (2011) Tightening of DNA knots by supercoiling facilitates their unknotting by type II DNA topoisomerases. Proc. Natl. Acad. Sci. USA 108, 3608–3611.
[14] Roca, J., Berger, J.M. and Wang, J.C. (1993) On the Simultaneous Binding of Eukaryotic DNA Topoisomerase-Ii to a Pair of Double-Stranded DNA Helices. J. Biol. Chem. 268, 14250–14255.
[15] Corbett, A.H., Zechiedrich, E.L. and Osheroff, N. (1992) A Role for the Passage Helix in the DNA Cleavage Reaction of Eukaryotic Topoisomerase-Ii - a 2-Site Model for Enzyme-Mediated DNA Cleavage. J. Biol. Chem. 267, 683–686.
[16] Binnig, G., Quate, C.F. and Gerber, C. (1986) Atomic force microscope. Phys. Rev. Lett. 56, 930–933.
[17] Hansma, P.K. et al. (1994) Tapping mode atomic-force microscopy in liquids. Appl. Phys. Lett. 64, 1738–1740.
[18] Kasas, S. et al. (1997) *Escherichia coli* RNA polymerase activity observed using atomic force microscopy. Biochemistry 36, 461–468.
[19] Muller, D.J. and Dufrene, Y.F. (2008) Atomic force microscopy as a multifunctional molecular toolbox in nanobiotechnology. Nat. Nanotechnol. 3, 261–269.
[20] Yaneva, M., Kowalewski, T. and Lieber, M.R. (1997) Interaction of DNA-dependent protein kinase with DNA and with Ku: biochemical and atomic-force microscopy studies. EMBO J. 16, 5098–5112.
[21] Trigueros, S., Arsuaga, J., Vazquez, M.E., Sumners, D.W. and Roca, J. (2001) Novel display of knotted DNA molecules by two-dimensional gel electrophoresis. Nucleic Acids Res. 29, E67-7.
[22] Zhang, P. et al. (2010) Engineering BspQI nicking enzymes and application of N.BspQI in DNA labeling and production of single-strand DNA. Protein Expr. Purif. 69, 226–234.
[23] Kasas, S., Alonso, L., Jacquet, P., Adamcik, J., Haeberli, C. and Dietler, G. (2010) Microcontroller-driven fluid-injection system for atomic force microscopy. Rev. Sci. Instrum. 81, 013704.
[24] Zechiedrich, E.L. and Osheroff, N. (1990) Eukaryotic topoisomerases recognize nucleic-acid topology by preferentially interacting with DNA crossovers. EMBO J. 9, 4555–4562.
[25] Osheroff, N. and Zechiedrich, E.L. (1987) Calcium-promoted DNA cleavage by eukaryotic topoisomerase II: trapping the covalent enzyme-DNA complex in an active form. Biochemistry 26, 4303–4309.
[26] Stone, M.D., Bryant, Z., Crisona, N.J., Smith, S.B., Vologodskii, A., Bustamante, C. and Cozzarelli, N.R. (2003) Chirality sensing by *Escherichia coli* topoisomerase IV and the mechanism of type II topoisomerases. Proc. Natl. Acad. Sci. USA 100, 8654–8659.
[27] Pietrement, O. et al. (2003) Reversible binding of DNA on NiCl2-treated mica by varying the ionic strength. Langmuir 19, 2536–2539.
[28] Berger, J.M., Gamblin, S.J., Harrison, S.C. and Wang, J.C. (1996) Structure and mechanism of DNA topoisomerase II. Nature 379, 225–232.
[29] Wei, H., Ruthenburg, A.J., Bechis, S.K. and Verdine, G.L. (2005) Nucleotide-dependent domain movement in the ATPase domain of a human type IIA DNA topoisomerase. J. Biol. Chem. 280, 37041–37047.
[30] Brino, L., Urzhumtsev, A., Mousli, M., Bronner, C., Mitschler, A., Oudet, P. and Moras, D. (2000) Dimerization of *Escherichia coli* DNA-gyrase B provides a structural mechanism for activating the ATPase catalytic center. J. Biol. Chem. 275, 9468–9475.
[31] Schultz, P., Olland, S., Oudet, P. and Hancock, R. (1996) Structure and conformational changes of DNA topoisomerase II visualized by electron microscopy. Proc. Natl. Acad. Sci. USA 93, 5936–5940.
[32] Nettikadan, S.R., Furbee, C.S., Muller, M.T. and Takeyasu, K. (1998) Molecular structure of human topoisomerase II alpha revealed by atomic force microscopy. J. Electron Microsc. 47, 671–674.
[33] Ando, T., Uchihashi, T., Kodera, N., Miyagi, A., Nakakita, R., Yamashita, H. and Sakashita, M. (2006) High-speed atomic force microscopy for studying the dynamic behavior of protein molecules at work. Jpn. J. Appl. Phys. 1-Reg. Pap. Brief Commun. Rev. Pap. 45, 1897–1903.
[34] Fantner, G.E., Hegarty, P., Kindt, J.H., Schitter, G., Cidade, G.A.G. and Hansma, P.K. (2005) Data acquisition system for high speed atomic force microscopy. Rev. Scient. Instrum. 76, 026118.
[35] Viani, M.B. et al. (2000) Probing protein–protein interactions in real time. Nat. Struct. Biol. 7, 644–647.